Journal of Physics:
Conference Series

PAPER • **OPEN ACCESS**

Analysis of crack formation mechanism in the wedge ring area of underwater high-speed vessels' shell

To cite this article: Tao Kong *et al* 2026 *J. Phys.: Conf. Ser.* **3175** 012139

Analysis of crack formation mechanism in the wedge ring area of underwater high-speed vessels' shell

Tao Kong[1,2*], Wenfeng He[1], Lei Wang[1], Jian Ma[1]

[1]Xi'an Precision Machinery Research Institute, Xi'an 710077, China
[2]Science and Technology on Underwater Information and Control Laboratory, Xi'an 710075, China

[*]Corresponding author's e-mail: 176212316@qq.com

Abstract. Wedge ring connections are commonly used for joining cylindrical sections in high-speed underwater vehicles. However, current research on wedge ring connections has not taken into account the stress problems under certain extreme conditions during operation, such as high-altitude transportation and vibration fatigue. These issues can lead to stress concentration in the shell's wedge ring area, resulting in the generation and propagation of cracks, posing serious safety hazards to product usage. Based on the working principle and load conditions of wedge rings, this paper conducts a non-linear finite element simulation analysis. It establishes the relationship between the wedge ring's condition during assembly and operation and the localized cracking of the shell. The results of the finite element analysis show good consistency with the actual crack conditions. This paper proposes improved design methods and assembly requirements for wedge ring connections to address the issue. The improved wedge ring structure and assembly requirements can significantly reduce stress concentration in the shell's wedge ring area under extreme conditions, effectively preventing the generation and extension of cracks.

1. Introduction

Wedge ring connections are commonly used for joining cylindrical sections in high-speed underwater vehicles. Compared to inclined screw connections, wedge ring connections offer several advantages: they eliminate the numerous holes on the shell surface between segmented structures that cause fluid disturbance and increase drag and noise for high-speed craft. Wedge ring connections are characterized by their compact structure, light weight, high space utilization, and smooth outer surface, which help maximize internal volume, reduce underwater or airborne flight resistance, and minimize fluid noise.

Many researchers have conducted extensive studies on wedge ring connections from various perspectives, including design, load conditions, vibration characteristics, and quality control. Chen et al. proposed improved methods for wedge ring design from a usage supportability standpoint [1]. Zou et al. developed a contact force prediction model based on multilayer perceptions to propose a method for detecting wedge ring installation forces, characterizing the compactness of assembly [2]. Huang et al. presented two finite element optimization schemes for wedge ring connections targeting maximum stress ratios [3]. Wang et al. studied how, during manufacturing, transportation, and service, cylindrical shells inevitably develop minor defects due to external factors, and under fatigue loading, small defects progressively grow with each load cycle [4]. Torabi and Alijani et al. investigated the buckling and vibration behaviors of functionally graded cylindrical panels with two distinct crack patterns under external pressure, and a semi-analytical finite element method was used considering various inclination angles, boundary conditions, and geometric parameters [5-6]. Wang et al. performed finite element analyses focusing on vibration performance, providing insights into shell vibration transmission and acoustic radiation characteristics using wedge ring connections [7]. Lv et al. analyzed the nonlinear buckling characteristics under axial compression of a cylindrical shell with axial and circumferential penetrating cracks [8]. Jahromi used the finite element method to study the influence of crack size and orientation on structural buckling behavior [9].

Despite extensive research efforts by scholars to improve wedge ring designs and manufacturing reliability, existing studies do not account for load conditions under certain extreme scenarios, such as high-altitude transportation or vibration fatigue. These conditions can lead to stress concentrations in the shell at the wedge ring area, potentially causing cracking and fracture risk. This study investigates the relationship between design parameters, assembly processes, and local shell cracking caused by wedge rings based on their working principles and nonlinear finite element simulations under extreme loading conditions. Improved design methods and assembly requirements for wedge ring structures are proposed accordingly.

2. Crack analysis in the window area of shell wedge ring

The cylindrical spacecraft with wedge ring connections, after undergoing high-altitude transportation and vibration fatigue, exhibited cracks of varying sizes on both sides of the shell's wedge ring connection window area, as shown in Figure 1. The crack morphology indicates that the cracks are of Type I (opening mode), caused by the tip opening under tensile stress perpendicular to the crack surface, and extending in a direction orthogonal to the applied tensile stress. Based on the analysis of the shell's loading conditions during high-altitude transportation, it is conjectured that under high-altitude vacuum conditions, the internal pressure of the product exceeds the external pressure, leading to tensile stress at the fillet of the shell's wedge ring connection. In extreme assembly configurations, this could result in significant stress concentration at the fillet, potentially exceeding the material's yield strength and causing cracks at the wedge ring opening.

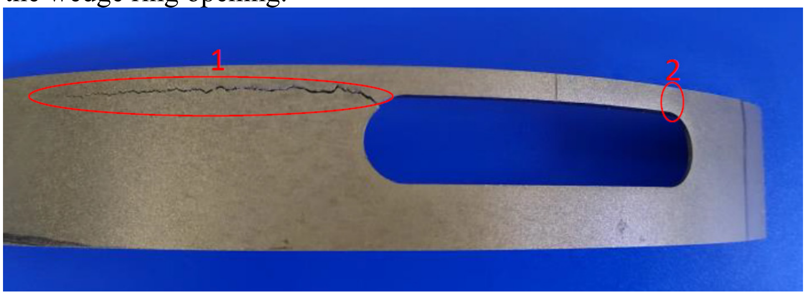

Figure 1. Crack fractures in the wedge ring window area after high-altitude transportation.

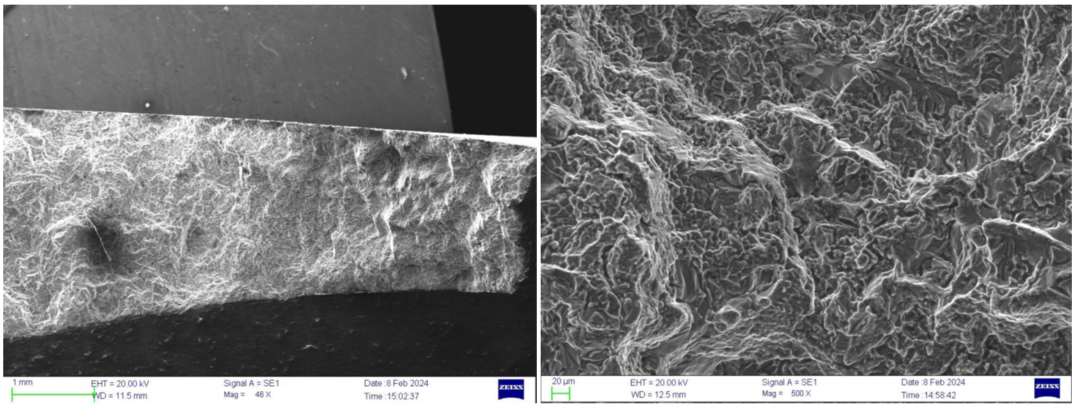

Figure 2. SEM examination results of fracture surfaces (46x on the right, 500x on the left).

A scanning electron microscopy (SEM) examination of the fracture surface was conducted, as shown in Figure 2. It was found that the fracture surface exhibited no obvious plastic deformation, indicating a brittle fracture. No significant blowholes, impurities, or porosity were observed on the

Journal of Physics: Conference Series **3175** (2026) 012139 doi:10.1088/1742-6596/3175/1/012139

fracture surfaces. The fracture morphology resembles that of a tension test sample, characterized by a mixture of dimple and quasi-cleavage features. Transverse cracks originated from the fillet within the wedge ring and expanded outward from the ring. Longitudinal cracks originated from the top of the wedge ring opening and extended upward. Both types of cracks resulted in a single fracture.

3. Stress state analysis of wedge ring connections

3.1. Wedge ring joint mechanical model

The structure of the wedge ring joint is illustrated in Figure 3. Two connected segments are fitted with an inner ring on the outer circumference of one segment and an outer ring on the inner circumference of the other segment. When these rings are coupled together, wedge ring grooves are formed on both rings, creating a circular cavity. The wedge bands are formed by bending two right-angled triangular metal strips, featuring a small wedge angle. One of these bands is equipped with a locating pin to become the locator wedge band. After coupling the inner and outer rings, the locator wedge band is inserted through a long circular hole on top of the wedge slot of the outer ring into the formed cavity, and the locating pin engages with the locating pin hole on the inner ring. During installation, two wedge bands are inserted into the wedge-shaped cavity from opposite sides of the shell's relative wedge windows, utilizing their relative motion to increase the assembly width and achieve a tight connection between the inner and outer shells.

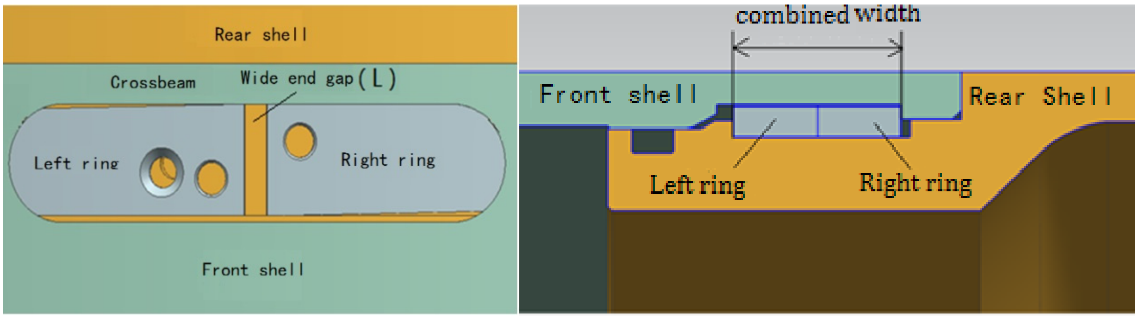

Figure 3. Assemblies of the wedge ring connection structure and two segments of the shell body.

According to the principle of wedge ring connection, the standard shell body assembly width for small-scale vessel segment connections is currently 18 mm, as shown in Figure 4. When two wedge rings are properly installed (due to manufacturing tolerances and usage wear, the width between their wide ends typically ranges from 15 mm to 40 mm), the axial assembly dimension of the wedge rings is set at 18 mm. In this configuration, the two wedge rings perfectly fill the assembly gap of the shell bodies, tightly securing the two segments so that they cannot separate. However, if the wedge rings are not installed correctly, as illustrated in Figure 5, they will fail to fully occupy the assembly gap of the shell bodies (which is 18 mm wide), resulting in a gap within the slot, as depicted in Figure 4.

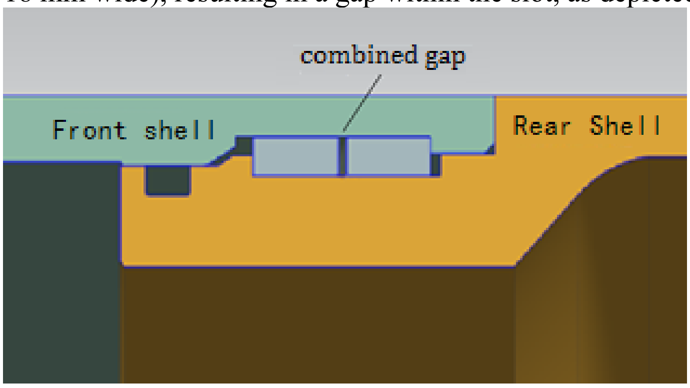

Figure 4. Illustration of the gap between wedge rings.

The relationship between the spacing of the wide ends of wedge rings (L) and their axial width after combination can be described by the following formula:

$$\Delta b = \Delta L \times \tan(\alpha) \tag{1}$$

where:

L is the spacing between the two wide ends of the wedge rings, mm.

ΔL is the change in width due to this spacing, mm.

b is the combined width when the wedge rings are assembled, mm.

Δb is the axial gap after assembly, mm.

a is the angle of the wedge ring's inclined surface.

According to standard GJB 819, which specifies that the wedge ring's inclined surface design angle a should be 1°3′ (1.05 degrees), substituting this value into the formula along with a desired axial gap Δb of 0.1 mm, we can calculate:

$$\Delta L = 2\times 1.05° \times 0.1 \ mm \approx 5.4 \ mm \tag{2}$$

This calculation indicates that when the wedge rings are assembled with an axial gap of 0.1mm and given the specified inclined angle, there will be a spacing of approximately 5.4 mm between their wide ends. In practical applications, this balance ensures that the vessel's structure remains secure while allowing for flexibility to accommodate operational conditions such as vibrations or thermal expansion. It also accounts for manufacturing tolerances and usage wear, contributing to the reliability and longevity of the connection.

3.2. Load conditions under high altitude negative pressure

Under high-altitude negative pressure conditions, the internal air pressure within the shell exerts an axial outward force on the contact surface between the shell and the wedge ring. The magnitude of this force is determined by the internal cross-sectional area of the shell and the internal pressure value.

To calculate the load F exerted around the circumference of the shell body's wedge ring, we use the following formula:

$$F = \pi\left(\frac{D}{2}\right)^2 \times P \tag{3}$$

where:

D is the internal diameter of the shell body, mm.

P is the pressure difference between inside and outside of the shell body, Pa.

For example, when the internal diameter D is 400 mm and the pressure difference P is 0.1 MPa, F is 12560 N. At this point, there is a tendency for the two shell bodies to separate, as illustrated in Figure 5. The red arrows in the figure indicate the direction of movement. However, the wedge rings counteract this separating trend by applying equal and opposite forces on both shells.

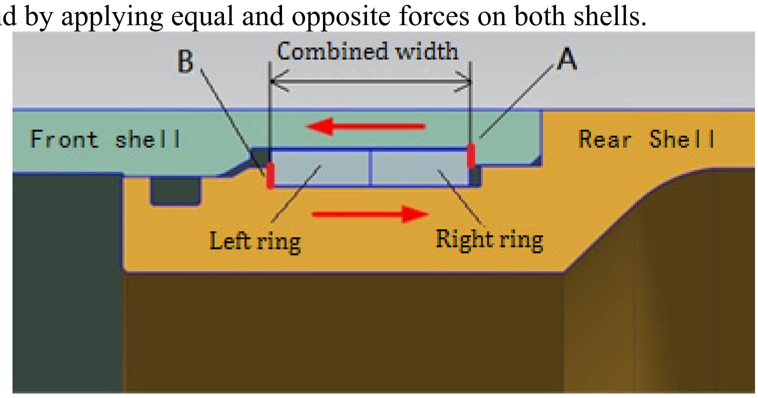

Figure 5. Forces and movement tendency of the shell under high-altitude vacuum conditions.

Since the Wedge Ring window position and the crossbeam form a single continuous surface, when subjected to internal gas pressure, the circular A-surface of the wedge ring groove experiences uniform loading between the wedge ring and the housing. The crossbeam surface must also withstand partial

Journal of Physics: Conference Series **3175** (2026) 012139 doi:10.1088/1742-6596/3175/1/012139

pressure from the wide end of the wedge ring. The crossbeam in the window area forms a fixed-fixed beam structure. The structural dimensions of the wedge ring ensure its wide end remains in contact with the crossbeam. Additionally, during assembly, the clearance at the wide end of the wedge ring is biased to one side, which will intensify the stress concentration at the window fillet radius on that side.

3.3. FEA of the stress state in wedge ring connection

In this section, we utilize the LS-Dyna nonlinear simulation module in Ansys finite element software to perform stress calculations for the shell under internal air pressure conditions. The load in the calculation process is a displacement load (combined gap Δb). Material parameters include aluminum alloy with an elastic modulus of 80 GPa, yield strength of 320 MPa, tensile strength of 340 MPa, and Poisson's ratio of 0.33.

Taking the extreme case of wedge ring assembly, where the spacing should be 38 mm but is currently at 6 mm, the axial matching gap between the two wedge rings is calculated to be 0.593 mm. This value is rounded to 0.6 mm as the displacement load is applied towards the left side of the window area. Displacement loads and boundary conditions are as illustrated in Figure 6; finite element grid division details are provided in Figure 7. Additionally, mesh refinement was conducted in the wedge ring window area with an average grid size of 0.25 mm.

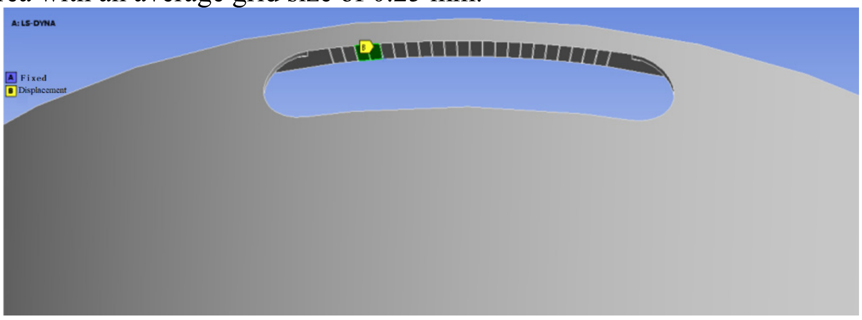

Figure 6. Fixed constraints at the far end of the shell body and displacement load application.

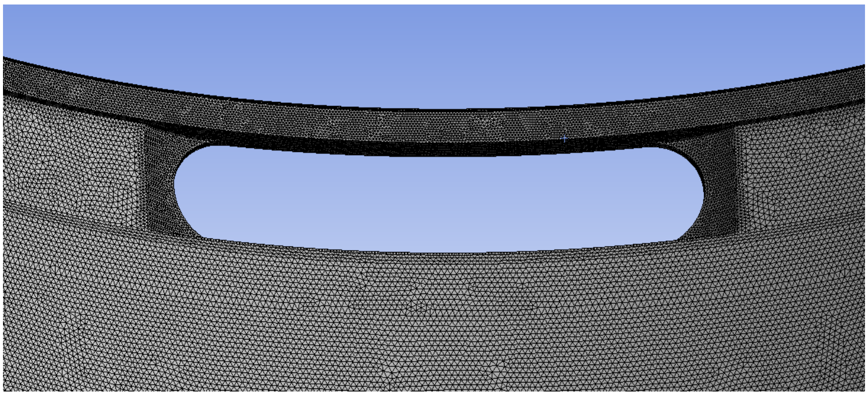

Figure 7. Mesh generation results in the wedge ring area.

Through calculation, the deformation cloud map of the shell wedge ring window area is shown in Figure 8(a), where the maximum deformation occurs at the top of the wide end of the wedge ring, with a deformation of 0.64 mm. The stress cloud map is illustrated in Figure 8(b), revealing that the maximum stress of 329 MPa appears on the upper half of the left circular corner, potentially leading to localized yielding at the wedge ring window fillet.

Considering special conditions such as vibrations, impacts, and temperature differences, when the displacement load is increased to 0.7 mm, the resulting deformation cloud map and stress cloud map are depicted in Figure 9. Under this load, a cracking phenomenon similar to that observed in faulty shells appears at the left circular corner of the shell window. The crack initiation point is at 9.3 mm from the

Journal of Physics: Conference Series **3175** (2026) 012139 doi:10.1088/1742-6596/3175/1/012139

segmentation face, which closely matches the actual value of 9.4 mm. The equivalent stress gradient map for the shell and wedge ring area is provided in Figure 10.

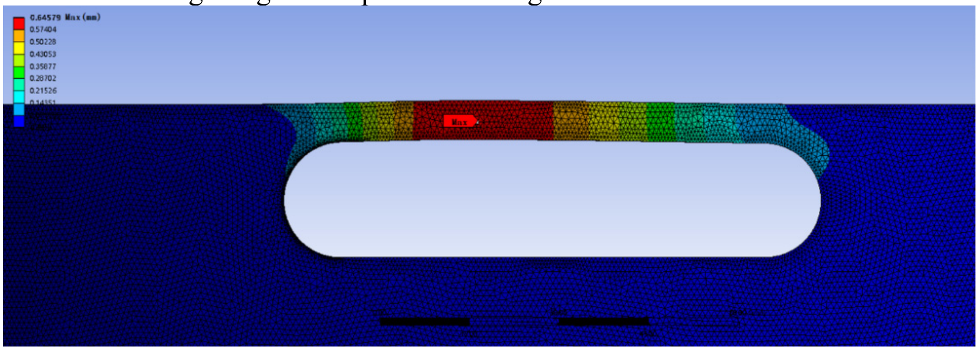

(a) Deformation cloud map

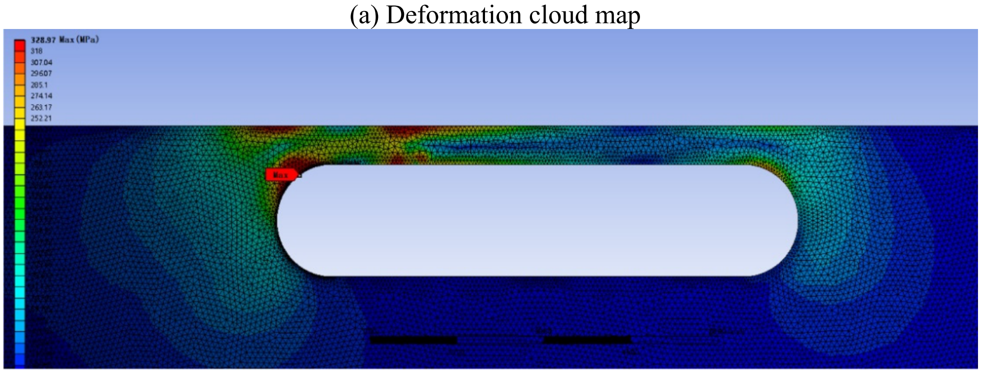

(b) Stress cloud map

Figure 8. Deformation and stress cloud map of the wedge ring window at 0.6 mm displacement load.

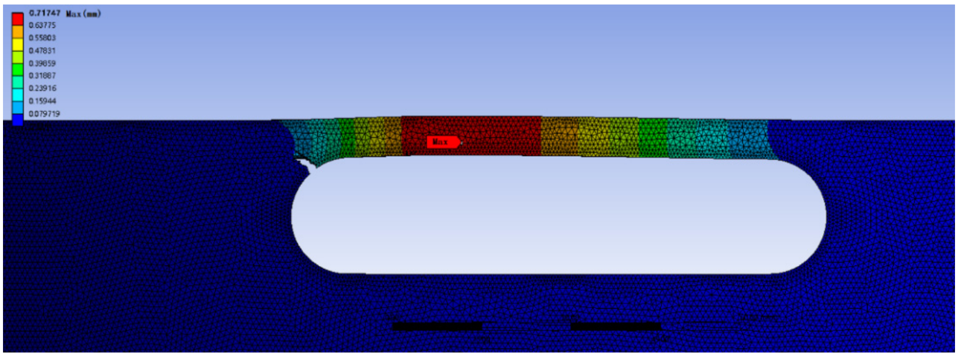

(a) Deformation cloud map

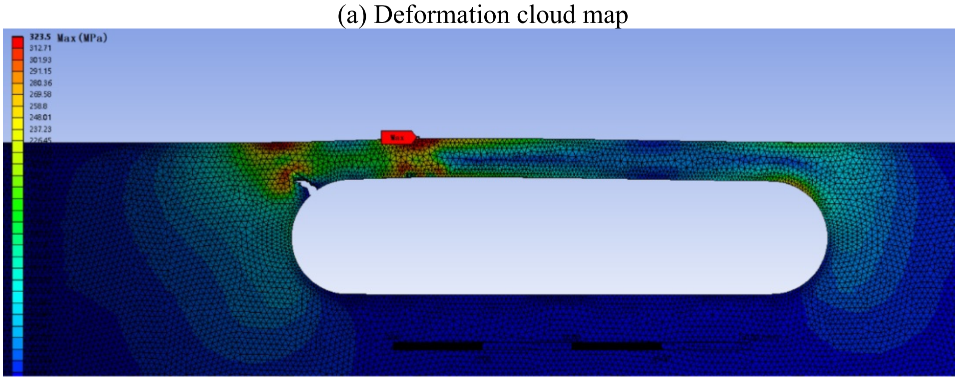

(b) Stress cloud map

Figure 9. Stress cloud map of the wedge ring window at 0.7 mm displacement load.

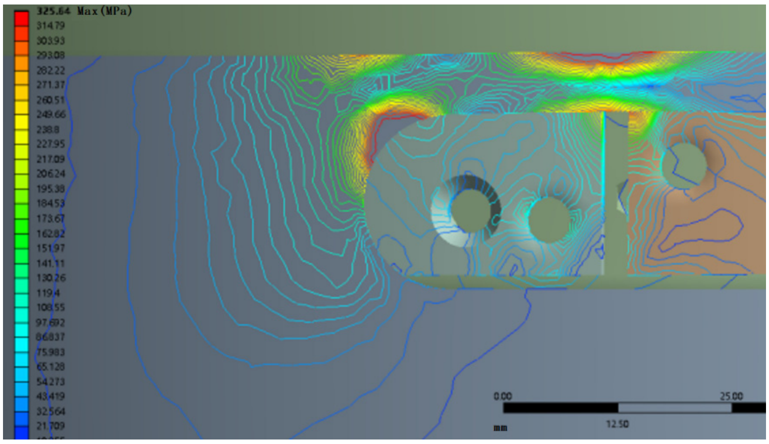

Figure 10. The equivalent stress gradient in the shell body wedge ring window area.

4. Conclusion

In this paper, based on the composition and usage principles of wedge rings and taking high-altitude transportation operating conditions as the foundation, we analyzed the formation mechanism of shell cracks encountered during wedge ring usage. Through nonlinear finite element analysis of extreme loading conditions, we found that some parameters of the wedge ring design were unreasonable, and improper installation further exacerbated the generation and propagation of cracks. Based on simulation results, we ultimately proposed two suggestions for wedge ring design and use. First, optimize the axial size of the large end of the wedge ring. Reducing the axial dimension by approximately 0.6 mm, without affecting its strength, can effectively reduce stress concentration in the wedge ring window area under high-altitude vacuum, vibration, and shock conditions. Second, standardize installation requirements for wedge rings and strictly control installation gaps to ensure uniform force on the inner wall of the shell and reduce the risk of cracking in weak areas.

References

[1] Chen S, Wang H, Li J, Liu J and Zhang J (2017) An Improved Design Method of Torpedo's Wedge Ring Connection Structure for Enhancement of Supportability, Journal of Unmanned Undersea Systems, 25: 371–376.
[2] Zou G, Sun P and Zhao Q, Huang H and Shen K (2024) Research on Total Contact Force Detection Method for Wedge Rind Based on Multilayer Perception, Drive System Technique, 38: 9–13.
[3] Huang P and Yin Y (2006) Two optimization designs research of wedged ring joint structure based on FEM, Chinese Journal of Mechanical Engineering, 42: 205–209.
[4] Wang S (2022), Structural strength analysis and residual life evaluation of cracked cylindrical shell, Harbin Engineering University, 5: 58–66.
[5] Torabi J and Ansari R (2020) Numerical investigation on the buckling and vibration of cracked FG cylindrical panels based on the phase-field formulation, Engineering Fracture Mechanics, 228: 106895.
[6] Alijani A, Barrera O and Bordas S (2021) Circumferential crack modelling of thin cylindrical shells in modal deformation, European journal of mechanics A/Solids, 90: 104360.
[7] Wang S, Yin S, Wang Z, Guo J and Zhang Z (2017) Study on Modal Characteristic of Torpedo Wedge ring Connection Structure, Journal of Unmanned Undersea Systems, 25: 453–458.
[8] Lv H, Zhu Y and Zhang S (2024) Research on nonlinear buckling of cylindrical shell with weld penetration crack under axial compression, Ship science and technology, 46: 127–131.
[9] Jahromi B H, Vaziri A (2012) Instability of cylindrical shells with single and multiple cracks under axial compression, Thin-Walled Structures, 54: 35–43.